3D Clay Printing: A Taguchi Approach To Rheological Properties And Printability Assessment

Nadir Rihani[1*], *Fatima-Zahra* Oulkhir[1], *Nnamdi* C. Igwe[1], *Iatimad* Akhrif[1], and *Mostapha* El Jai[1,2]

[1]Euromed University of Fes, UEMF, Morocco.
[2]ENSAM-Meknes, Moulay Ismail, University, Meknes, Morocco.

Abstract. In the general context of 3D clay printing and sustainable mix design, reaching optimal printing quality and structural integrity requires a thorough understanding of the fresh paste and solid properties of earthen materials. This study investigates the rheology of Benjellik clay using Taguchi Design plan, focusing on the effects of particle size and water content on the related fresh paste properties. A set of nine clay formulations were analysed in terms of yield stress, plastic viscosity, consistency, and flow number according to both Bingham and Bulkley models. Results revealed that water to binder ratio (W/B) mainly impacts rheological properties; it reduces yield stress and plastic viscosity while increasing the flow number. Moreover, the pre-selected raw particle sizes had irrelevant impact due to similarities of the related statistical distributions as corroborated by laser granulometry tests. Furthermore, optimal layer heights to nozzle diameter ratio was found to be around 0.55 enhancing the material flowability and scanned tracks features. Finally, the findings emphasize the crucial role of W/B along with the layer height to nozzle size ratios in stabilizing the printability of clay materials, offering a confident printing parameters area for optimizing both 3D printing clay of Fez region of Morocco.

1 Introduction

The advent of additive manufacturing, commonly referred to as 3D printing, has revolutionized various industries by enabling the production of complex geometries [1] with a high degree of precision [2–4] and minimal waste [5–7]. Among the various materials used for 3D printing, clay has garnered significant attention due to its accessibility, sustainability, and historical significance in human craftsmanship. In particular, 3D clay printing has opened new avenues in art, architecture, and engineering, allowing for the creation of intricate and customized ceramic structures [8,9].

One critical aspect of 3D clay printing is the rheological behavior of the clay paste, which determines its printability, shape retention, and final mechanical properties. Rheology, the study of the flow and deformation of matter, is particularly important in 3D printing as it

* Corresponding author: n.rihani@ueuromed.org

affects the material's ability to be extruded smoothly through the printer nozzle and to maintain its shape after deposition [10–12]. The rheological properties of clay slurries are influenced by several factors, including the particle size distribution of the clay powder, the concentration of solid particles, and the presence of additives [10,11].

Marl, a type of calcareous clay, is commonly used in ceramic production and has recently been explored for 3D printing applications. The particle size of marl powder can significantly impact the rheological properties of the paste. Smaller particles tend to increase the slurry's viscosity and yield stress due to their larger surface area and higher interaction forces, while larger particles may lead to a more fluid slurry with lower yield stress [13,14]. Understanding the relationship between particle size and rheological behavior is essential for optimizing the printing process and achieving high-quality printed objects.

The rheological behavior of clay pastes is complex and depends on the interplay of various factors, including particle size distribution, solid content, and the presence of dispersants or binders. Rheological models, such as the Herschel-Bulkley model [15] expressed in eq (1), are commonly used to describe the flow behavior of clay pastes. The Herschel-Bulkley model is a three-parameter model that accounts for yield stress, consistency, and shear-thinning behavior [15,16].

$$\tau = \tau_0 + K\,\dot{\gamma}^n \quad (1)$$

Where τ is the shear stress, τ_0 is the yield stress, K is the consistency index, $\dot{\gamma}$ is the shear rate, and n is the flow behavior index. The Bingham plastic model, on the other hand, is a simpler two-parameter model that describes materials with a linear relationship between shear stress and shear rate once the yield stress is exceeded [16,17]. The model is expressed in eq (2).

$$\tau = \tau_0 + \eta_p\dot{\gamma} \quad (2)$$

Where τ is the shear stress, τ_0 is the yield stress, η_p is the plastic viscosity, $\dot{\gamma}$ is the shear rate.

2 Materials and methods

2.1 Marl presentation and preparation

Benjellik clay, sourced from a region near Fez, Morocco, is notable for its unique composition and properties. This material, also referred to as marl, is extensively studied for various applications, including construction, ceramics, and advanced material composites. The following subsections provide an overview of its physico-chemical, mechanical, rheological properties.

2.1.1 Physico-Chemical Properties

Benjellik clay, a Miocene marl, is characterized by its light color (yellow to gray) and fine-grained texture. The mineralogical composition primarily includes kaolinite, illite, calcite, and quartz [18–20]. The carbonate content is relatively high, approximately 34% as measured using Bernard's calcimeter. Moreover, X-ray diffraction (XRD) analysis confirms the presence of kaolinite, illite, quartz, and calcite as major crystalline components. Peaks for these minerals are significant in the XRD patterns [21]. Furthermore, the chemical analysis using Inductive Coupled Plasma (ICP) shows substantial amounts of silicon dioxide (SiO_2), aluminum oxide (Al_2O_3), iron oxide (Fe_2O_3), calcium oxide (CaO), and magnesium oxide (MgO). Specific values are SiO_2 (49.50% - 49.60%), Al_2O_3 (14.50% - 22.60%), CaO (0.12% - 12.14%), Fe_2O_3 (2.88% - 4.63%), and MgO (2.18% - 3.62%) [22].

2.1.2 Mechanical Properties

The mechanical properties of Benjellik clay, especially when mixed with Polyethylene Glycol (PEG 6000), have been previously studied to enhance its applications:

- **Elasticity and Plasticity**: Addition of PEG 6000 increases both elasticity modulus and plasticity. The Young modulus values oscillate around an average value of 400 MPa, showing a significant increase with the fineness of grinding, suggesting better particle agglomeration. The values for Young's modulus range from approximately 300 MPa to 500 MPa, depending on the grinding size and PEG concentration [21].
- **Strength:** The mechanical strength, measured as the maximum stress the material can withstand, shows values oscillating around the initial values of the raw clay material, approximately 25 KN. The mechanical strength does not show significant evolution with different grinding sizes and PEG concentrations [21].

2.1.3 Pre-processing

For this study, marl powder is essential for rheology tests. Benjellik marl is processed into powder through several steps: extraction from the Benjellik quarry, hammer crushing, drying to remove moisture, initial grinding in a grinding pot, refined grinding with a Retsch automatic grinder, sieving to separate grain sizes, and storage. Figure Fig. 1 illustrates the various granulometry sizes of the powder (90 µm, 125 µm, and 212 µm).

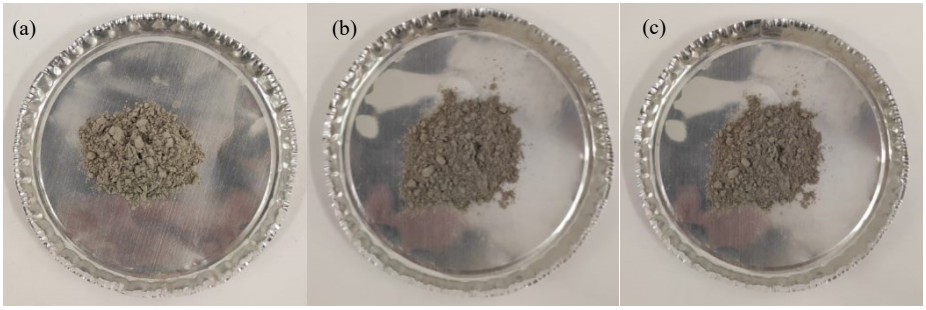

Fig. 1. Marl powder, (a) G090, (b) G0125, (c) G0212.

2.2 Taguchi DoE and 3D Clay printing

To systematically investigate the effects of water content and particle size on the rheological properties of Benjellik marl clay, a Taguchi Design of Experiments (DoE) was employed [23]. This robust statistical approach optimizes the experimental process by examining multiple factors at different levels with a minimal number of experiments. The study utilized two factors: particle size (90 µm, 125 µm, and 212 µm) and water content (33.33%, 37.50%, and 41.67%) at three levels each, resulting in nine unique formulations. Each formulation was subjected to rheological testing to determine key parameters such as yield stress (τ_0), plastic viscosity (η_p), consistency (K), and flow number (n). The tests were conducted using a parallel plate rheometer, and the rheological data were analysed using both Bingham and Bulkley models to capture any linear and non-linear behaviors, respectively. Based on the rheological parameters, the best and worst-performing samples were identified. The formulation with the highest yield stress, indicating the highest resistance to initial flow, was selected as the best sample. Conversely, the sample with the least yield stress and plastic viscosity was identified as the worst performer.

To further explore the practical applications of the selected formulations, the best and worst samples will be printed into 2D shapes. These printing trials aim to fine-tune the layer height parameter, a crucial factor in achieving optimal print quality and structural integrity. The 2D printing tests will provide insights into how the rheological properties translate into printability and the quality of printed layers.

3 Results and discussion

3.1 Rheological tests

Rheology tests are critical for characterizing the flow and deformation behavior of clay materials in 3D printing applications. These tests provide essential insights into the viscoelastic properties of clay, which directly impact the printability, structural integrity, and surface finish of printed objects. In this work, the rheological tests were conducted using a parallel plate rheometer. The test consists of placing the clay sample between two flat, parallel plates. During the test, 60 measurement points corresponding to different shear rates ranging from 0.1 to 100 s^{-1} were taken over the course of 1 minute. The test assumes that the clay sample is homogeneous, isotropic, and adheres to a non-slip boundary condition with the plates, with flow reaching a steady state.

Fig. 2 presents the shear stress (τ) versus shear rate ($\dot{\gamma}$) curves for various clay samples labelled TAG2, TAG3, TAG4, TAG5, TAG6, TAG8, and TAG9. The rheological curves were generated using the parallel plate rheometer under the shear rate conditions described earlier. The data illustrates the relationship between shear stress and shear rate for each sample, highlighting the non-Newtonian behavior of the clay materials. It is noteworthy that during the tests, samples TAG1 and TAG7 exhibited excessive strength due to low water content. This resulted in such high reaction forces that the rheometer stopped the tests to prevent potential damage to its load cell.

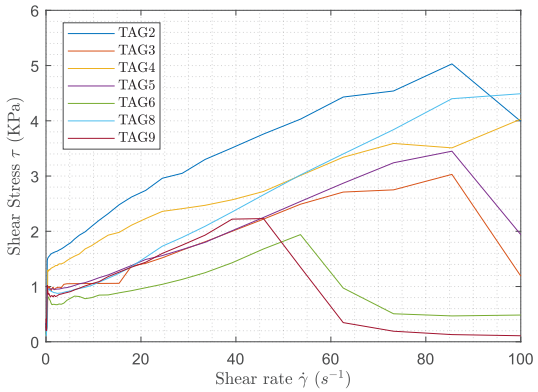

Fig. 2. Rheology test outputs.

3.2 Bingham's plastic model fitting

In the experimental rheological data, a likely linear relationship is observed between the shear stress (τ) versus shear rate ($\dot{\gamma}$), suggesting a Bingham plastic model. Hence, linear fittings were conducted on the linear region of each sample's rheology as depicted in Fig. 3. The fittings revealed a highly significant dependency between shear rate and shear stress, with coefficients of determination (R-squared) ranging from 96% to 99%, and p-values ranging from 1.23E-39 to 7.24E-17, well below the 10^{-5} statistical significancy threshold [24]. The related Table 1 depicts the detailed Bingham's model fitting results, including the sample's particle size class and water to binder ratio (W/B), the corresponding rheological parameters (yield stress (τ_0) and plastic viscosity (η_p), and the related statistical indicators (R-squared values, and p-values).

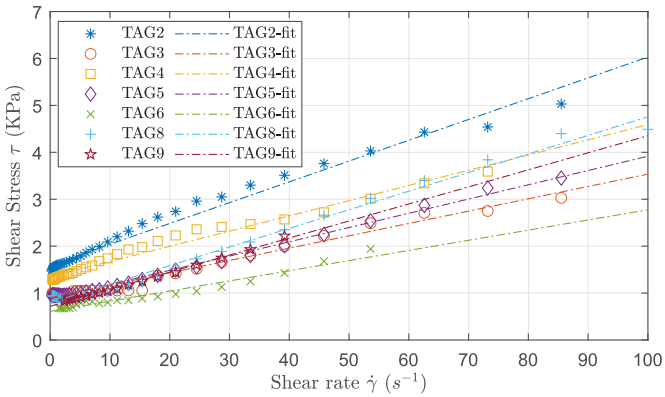

Fig. 3. Bingham model fittings.

Table 1. Bingham model fitting results.

Sample	Sieving class (µm)	W/B ratio	Yield stress τ_0 (Pa)	Plastic viscosity η_p (Pa.s)	R-Squared	p-Values
TAG 1	212	33.33%	N.A	N.A	N.A	N.A
TAG 2	212	37.50%	1598	44	0.980	2.87E-32
TAG 3	212	41.67%	906	26	0.978	7.05E-30
TAG 7	125	33.33%	N.A	N.A	N.A	N.A
TAG 8	125	37.50%	794	40	0.987	7.45E-36
TAG 9	125	41.67%	720	36	0.995	3.75E-21
TAG 4	90	33.33%	1349	32	0.978	5.41E-29
TAG 5	90	37.50%	877	30	0.993	1.23E-39
TAG 6	90	41.67%	610	22	0.960	7.24E-17

3.3 Herschel-Bulkley's model fitting

While the Bingham model revealed a confirmed linear relationship between shear stress and shear rate, the Bulkley model was employed to investigate further any potential non-linearity observed in the rheological data. Non-linear fittings were conducted on each sample's rheology curve as plotted in Fig. 4. The fittings revealed a significant dependency between shear rate and shear stress, with the model parameters including yield stress, consistency, and flow number. The related Table 2 depicts the detailed Bulkley model fitting results, including the sample's particle size class and water content, the corresponding rheological parameters (yield stress (τ_0), consistency (K), and flow number (n), and the related statistical indicators (R-squared values and RMSE).

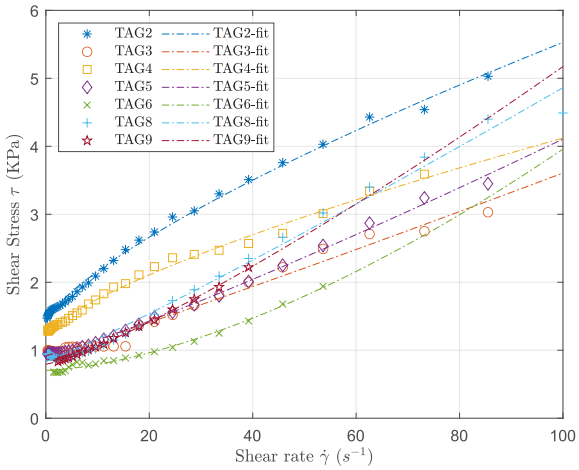

Fig. 4. Bulkley model fittings.

Table 2. Herschel-Bulkley's fitting results.

Sample	Yield stress τ_0 (Pa)	Consistency K (Pa.s^n)	Flow number (n)	R-Squared	RMSE
TAG 1	N.A	N.A	N.A	N.A	N.A
TAG 2	1412	136.3	0.74	0.976	0.054
TAG 3	925.2	19.97	1.064	0.987	0.057
TAG 7	N.A	N.A	N.A	N.A	N.A
TAG 8	834.1	27.36	1.084	0.981	0.052
TAG 9	793.7	16.57	1.211	0.995	0.041
TAG 4	1217	98.84	0.7346	0.968	0.045
TAG 5	919.4	16.88	1.138	0.993	0.067
TAG 6	704.6	2.283	1.577	0.962	0.053

3.4 Water content and particle size effects

Interpreting the rheological test results requires careful consideration of the effects of water content and particle size on yield stress, plastic viscosity, and flow behavior. The study employs the Taguchi method with two factors (particle size and water content) at three levels to systematically explore their effects on both Bingham's and Bulkley's model fitting coefficients. While ANOVA is typically used to analyse statistical significance [25,26], its application herein is limited due to missing data and its inefficacy in capturing the complex, non-linear relationships in rheological properties.

3.4.1 Water content effect

The water content significantly impacts both the yield stress and plastic viscosity of the clay samples. Higher water content reduces the interparticle interactions, leading to lower yield stress and plastic viscosity. This is due to the increased lubrication between particles, which facilitates easier flow and deformation.

- *Water content effect on yield stress* τ_0

Yield stress decreases significantly with increasing water content across all particle sizes. For the 212 µm grain size class, the yield stress dropped by 43.28% when the water content increased from 37.50% to 41.67%. Similarly, for the 90 µm particle size, it decreased by

30.44%. This suggests that higher water content reduces inter-particle interactions, resulting in a slurry that is less resistant to flow.

- *Water content effect on plastic viscosity* η_p

Plastic viscosity also diminishes with higher water content. For the 212 μm grain size, viscosity reduced by 40.68%, and for the 90 μm particle size, it decreased by 28.77%. The increased water content provides better lubrication between particles, reducing internal friction and thus lowering the viscosity.

- *Water content effect on consistency (K)*

Consistency, representing the material's thickness, decreases with increasing water content. For instance, TAG 2 with 37.50% water content shows a consistency of 136.3, which drops to 19.97 for TAG 3 with 41.67% water content. This indicates that higher water content reduces the internal resistance of the clay, making it less viscous and more flowable.

- *Water content effect on flow number (n)*

The flow number, which characterizes the flow behavior under applied stress, increases with higher water content. TAG 2 has a flow number of 0.74, while TAG 3 has 1.064, indicating a transition from more solid-like to fluid-like behavior. This aligns with findings in the literature, where water content is shown to play a crucial role in modifying the rheological properties of clays.

The interactions between clay particles are primarily driven by electrostatic forces, van der Waals forces, and hydration layers. As water content increases, the hydration layers around the clay particles expand, reducing the effective particle-particle interactions and leading to lower yield stress and plastic viscosity. This is consistent with findings in the literature, where increased water content diminishes the attractive forces between particles, enhancing flowability and reducing resistance to shear strains [27–29].

At a microscale level, higher water content results in a more dispersed particle arrangement, reducing the formation of a continuous particle network that resists flow. This dispersion effect lowers both yield stress and plastic viscosity. Conversely, lower water content leads to tighter particle packing and stronger interparticle networks, increasing resistance to flow and enhancing yield stress and plastic viscosity; in this context, Zheng et al investigated [30] illustrates scanning electron microscopy SEM images of clayey loess soil specimens with various water contents, highlighting their microstructural evolution. In the drying path, at high water content, clay particles are fully hydrated and form weak 'floc' structures, resulting in low resistance due to point–point particle contacts and mosaic pores. As water content decreases, clay particles aggregate into bridges and buttresses, filling inter-particle pores and enhancing strength. At low water content, increased clay cementation firmly bonds particles, reducing pores and stabilizing the soil fabric.

3.4.2 Particle size effect

In this study, the particle size effect on yield stress and plastic viscosity appears to be insignificant. This can be attributed to the dominant influence of water content over particle size in determining the rheological properties of the clay. The particle size classes (90 μm, 125 μm, and 212 μm) do not show a similar trend in affecting the rheological parameters, suggesting that within the studied range, particle size has a minor impact compared to water content. Typically, one would expect smaller particle sizes to increase yield stress and plastic viscosity due to a higher surface area-to-volume ratio, leading to more particle-particle interactions and stronger network structures within the clay matrix. However, the results indicate that the variations in water content overshadow these size effects, likely due to the significant role of hydration in modulating the clay's microstructure and interparticle bonding, thereby governing its overall rheological behavior.

Despite observing a non-significant impact of particle size on the rheological properties in this study, additional investigations into particle size distributions were carried out using laser granulometry. The apparatus used for this analysis was the particle size and shape analyser MICROTRAC CAMSIZER X2. The results of the particle size distribution analysis were fitted to a log-normal distribution expressed in expression (3), results indicate that the particle size distributions of the clay samples conform well to a log-normal distribution (see Fig. 5), as evidenced by the high R-squared values (ranging from 0.873 to 0.910) and low RMSE values (ranging from 0.0021 to 0.0027) presented in table 3. The μ values, representing the mean particle size on a log scale, are relatively close across the different powder samples, with slight variations (3.468 μm for G0212, 3.252 μm for G0125, and 3.058 μm for G090). The standard deviations σ are also approximatively similar (1.271 for G0212, 1.092 for G0125, and 1.145 for G090). The mean sphericity and symmetry ratios are similar across the samples, reveling that the shape of the particles does not vary significantly with different sieving sizes The results also indicate a significant sphericity above 82% and a high symmetry ratio above 90%.

$$y = \frac{1}{x\sigma\sqrt{2\pi}} \exp\left(-\frac{(\ln x - \mu)^2}{2\sigma^2}\right) \tag{3}$$

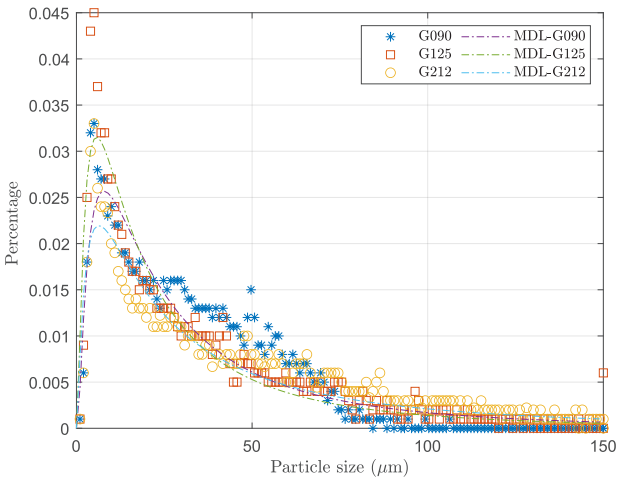

Fig. 5. Particle size distribution.

The analysis of particle size distribution shows that despite using different sieving diameters (90 μm, 125 μm, and 212 μm), the particle size distribution parameters and shape ratios are almost identical. This suggests that the sieving process may not effectively separate fine grains. These conclusions explain the non-significant impact of grain size on the clay's rheological properties. The dominant influence of water content further overshadows any subtle effects of particle size distribution.

Table 3. Particle size and shape indicators.

	Lognormal fitting				Distribution's indicators		Particle's shape ratios	
Sieve size	**Mean μ (μm)**	**Standard deviation σ**	**R squared**	**RMSE**	**Skewness**	**Kurtosis**	**Mean Sphericity ratio**	**Mean Symmetry ratio**
G-212	3.468	1.271	0.8819	0.0027	1.8786	7.1969	0.835	0.904
G-125	3.252	1.092	0.9105	0.0025	2.258	8.7366	0.822	0.905
G-090	3.058	1.145	0.8731	0.0021	1.093	3.4966	0.825	0.907

3.5 3D clay printing

The 3D clay printing experiments involved printing square-shaped contours with different fillet angles using various layer heights (1.5 mm, 2 mm, 2.5 mm, and 3 mm) as depicted in the Appendix. The printing was performed with a nozzle diameter of 5 mm and a scan speed of 1500 mm/min. The goal is to fine-tune the layer height parameter to reach optimal print quality and structural integrity for the best and worst-performing clay formulations: TAG2 (best sample: 212 µm particle size, 37.50% water content) in contrast with TAG6 prints (one of the lesser performing samples: 90 µm particle size, 41.67% water content).

The freshly printed samples demonstrate varying levels of stability and quality. Figure Fig. 8(a) shows the freshly printed TAG6, which features smooth layers but suffers from instability and unevenness due to its lower yield stress and plastic viscosity. In contrast, Fig. 8(b) illustrates the freshly printed TAG2, which has well-defined, stable layers with minimal deformation, reflecting its higher yield stress and structural integrity. A side view of the freshly printed TAG2 in Fig. 8(e) further highlights its consistency and stability, showcasing superior print quality compared to TAG6. When dried, the samples reveal more about their structural properties. Fig. 8(c) shows the dry TAG6, which exhibits noticeable shrinkage and deformation, indicating weaker structural stability due to its lower rheological properties. Conversely, Fig. 8(d) displays the dry TAG2, which maintains its structural integrity with minimal shrinkage, attributed to its higher yield stress and plastic viscosity, ensuring quality post-drying.

The experiments identified that the best layer heights for this nozzle diameter (5 mm) are between 2.5 mm and 3 mm. This range produced the most stable and well-defined layers, balancing the flow of material and the structural integrity of the printed shapes. These findings are consistent with the z/d ratios reported in the literature [31–34]. which suggest that optimal layer heights are proportional to the nozzle diameter to deliver high-quality prints.

4 Conclusion

This study systematically explored the rheological properties of Benjellik marl clay using the Taguchi Design of Experiments (DoE) methodology, focusing on the particle size and water content effects. On the one hand, higher water content significantly reduced yield stress, plastic viscosity, and consistency, while increasing the flow number, facilitating easier flow and deformation. On the other hand, the impact of particle size was minimal, overshadowed by the dominant influence of water content. TAG2 (212 µm particle size, 37.50% water content) emerged as the best-performing sample with the highest yield stress, while TAG6 (90 µm particle size, 41.67% water content) was one of the least-performing samples. Furthermore, additional laser granulometry analysis confirmed similar particle size characteristics across different grain sizes. 3D printing trials indicated optimal layer heights of 2.5 mm to 3 mm for a 5 mm nozzle, reaching a good balance of material flow and structural integrity. Future works will focus on buildability and infill strategies investigations.

References

1. M. El Jai, I. Akhrif, and N. Saidou, Prog Addit Manuf **6**, 781 (2021)
2. K. Fri, I. Akhrif, A. Laazizi, M. El Jai, M. Bensada, and A. Ouannou, Prog Addit Manuf (2023)
3. K. Fri, A. Laazizi, I. Akhrif, M. E. Jai, A. Ouannou, and M. Bensada, in *Advances in Integrated Design and Production II*, edited by L. Azrar, A. Jalid, S. Lamouri, A.

Siadat, M. Taha Janan, F. Chaari, and M. Haddar (Springer International Publishing, Cham, 2023), pp. 500–508
4. K. Fri, A. Laazizi, M. Bensada, M. E. Alami, A. Ouannou, I. Akhrif, M. E. Jai, and J. Fajoui, Int J Adv Manuf Technol **124**, 2289 (2023)
5. X. Wang, W. Li, Y. Guo, A. Kashani, K. Wang, L. Ferrara, and I. Agudelo, Developments in the Built Environment **17**, 100378 (2024)
6. N. Rihani, I. Akhrif, and M. El Jai, Frontiers of Architectural Research **13**, 650 (2024)
7. M. El Jai, N. Saidou, M. Zineddine, and H. Bachiri, Prog Addit Manuf **6**, 93 (2021)
8. J. Alonso Madrid, G. Sotorrío Ortega, J. Gorostiza Carabaño, N. O. E. Olsson, and J. A. Tenorio Ríos, Crystals **13**, 375 (2023)
9. N. Rihani, I. Akhrif, M. E. Jai, and M. Lamghari, Statistics, Optimization & Information Computing **12**, 713 (2024)
10. M. K. Mohan, A. V. Rahul, K. Van Tittelboom, and G. De Schutter, Cement and Concrete Research **139**, 106258 (2021)
11. A. U. Rehman and J.-H. Kim, Materials **14**, 3800 (2021)
12. K. El Abbaoui, I. Al Korachi, M. El Jai, B. Šeta, and Md. T. Mollah, Journal of Manufacturing Processes **118**, 448 (2024)
13. S. Kaushik, M. Sonebi, G. Amato, A. Perrot, and U. K. Das, Materials Today: Proceedings **58**, 1063 (2022)
14. E. M. Aydin, B. Kara, Z. B. Bundur, N. Ozyurt, O. Bebek, and M. Ali Gulgun, Construction and Building Materials **350**, 128935 (2022)
15. W. H. Herschel and R. Bulkley, Kolloid-Zeitschrift **39**, 291 (1926)
16. T. G. Mezger, *The Rheology Handbook: For Users of Rotational and Oscillatory Rheometers* (Vincentz Network GmbH & Co KG, 2006)
17. E. C. Bingham, *Fluidity and Plasticity.* (McGraw-Hill, New York, 1922)
18. I. Akhrif, M. E. Jai, L. Mesrar, and R. Jabrane, OJCE **06**, 577 (2016)
19. I. Akhrif, L. Mesrar, M. E. Jai, M. Benhamou, and R. Jabrane, (n.d.)
20. I. Akhrif, M. El Jai, L. Mesrar, A. Elkhalfi, A. Touache, and R. Jabrane, ENG **06**, 338 (2014)
21. M. E. Jai, I. Akhrif, L. Mesrar, and R. Jabrane, IOP Conf. Ser.: Mater. Sci. Eng. **353**, 012015 (2018)
22. L. Mesrar, M. Akdim, M. Lakrim, O. E. Aroussi, I. Akhrif, and R. Jabrane, Present Environment and Sustainable Development **9**, 103 (2015)
23. G. Dong, G. Wijaya, Y. Tang, and Y. F. Zhao, Additive Manufacturing **19**, 62 (2018)
24. J. P. Simmons, L. F. Drummy, C. A. Bouman, and M. D. Graef, editors , *Statistical Methods for Materials Science: The Data Science of Microstructure Characterization* (CRC Press, Boca Raton, 2019)
25. S. Kim, J. Jang, and O. Kim, Polymer Testing **17**, 225 (1998)
26. S. Maghsoodloo, G. Ozdemir, V. Jordan, and C.-H. Huang, Journal of Manufacturing Systems **23**, 73 (2004)
27. W. Markgraf, R. Horn, and S. Peth, Soil and Tillage Research **91**, 1 (2006)
28. R. Jayathilakage, P. Rajeev, and J. Sanjayan, Cement and Concrete Composites **121**, 104075 (2021)
29. J. Huang, L. Wang, T. Li, and J. Shao, Textile Research Journal **88**, 614 (2018)
30. P. Zheng, J. Wang, Z. Wu, W. Huang, C. Li, and Q. Liu, Applied Sciences **12**, 8470 (2022)
31. K. Ouazzani, M. el Jai, I. Akhrif, M. Radouani, and B. el Fahime, The International Journal of Advanced Manufacturing Technology **127**, 1 (2023)
32. K. Ouazzani, M. E. Jai, and B. Elfahime, in *2022 2nd International Conference on Innovative Research in Applied Science, Engineering and Technology (IRASET)* (2022), pp. 1–9

33. K. Ouazzani, I. Akhrif, N. Rihani, M. E. Jai, M. Radouani, and B. E. Fahime, Moroccan Journal of Chemistry **12**, 1621 (2024)
34. K. Ouazzani, M. E. Jai, I. Akhrif, M. Radouani, and B. Elfahime, in *2024 4th International Conference on Innovative Research in Applied Science, Engineering and Technology (IRASET)* (2024), pp. 1–5

Appendix

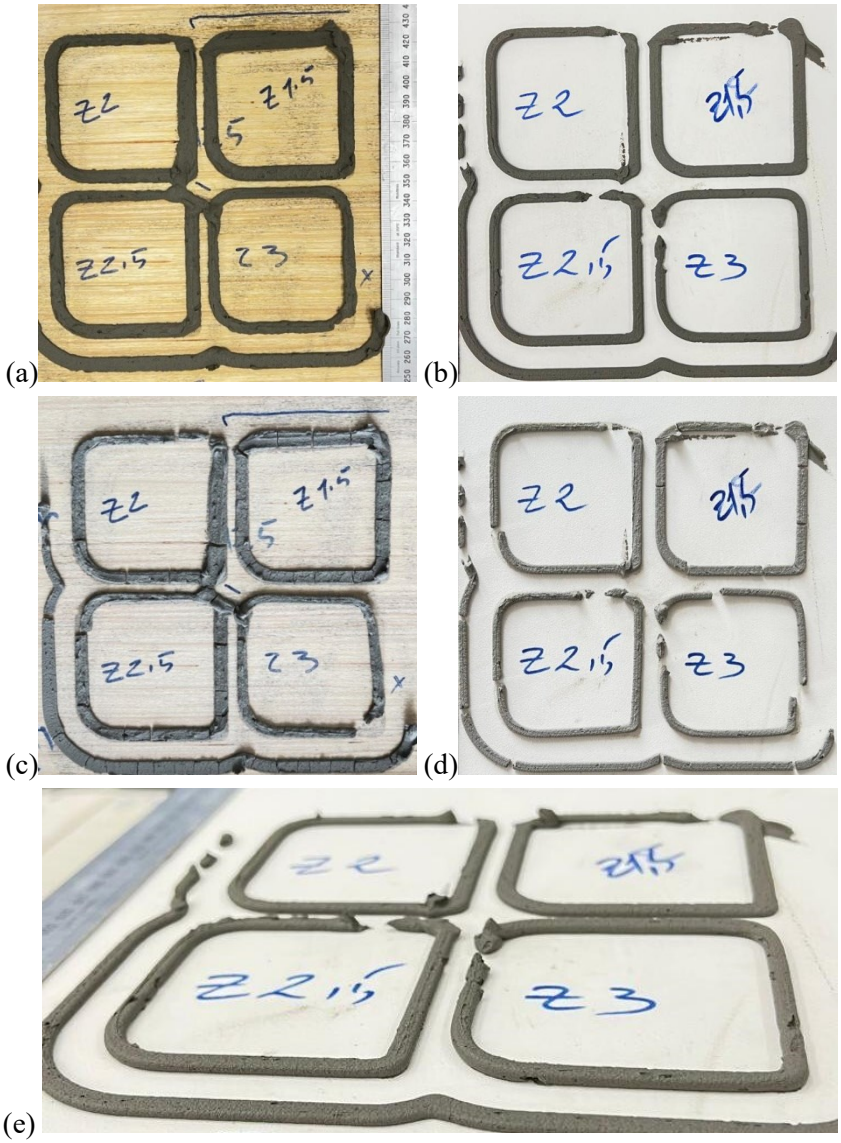

Fig. 6. Layer height fine-tuning, (a) freshly printed TAG6 mix sample, (b) freshly printed TAG2, (c) dry TAG6, (d) dry TAG2, (e) freshly printed TAG2 side view.